Available online at www.sciencedirect.com
ScienceDirect
Journal of Sound and Vibration 305 (2007) 703–727
JOURNAL OF SOUND AND VIBRATION
www.elsevier.com/locate/jsvi

Fixed points on the nonlinear dynamic properties of hydraulic engine mounts and parameter identification method: Experiment and theory

Ranglin Fan*, Zhenhua Lu

State Key Laboratory of Automotive Safety and Energy, Department of Automotive Engineering, Tsinghua University, Beijing 100084, PR China

Received 18 April 2006; received in revised form 7 March 2007; accepted 21 April 2007
Available online 13 June 2007

Abstract

Of the various types of passive engine mounts, hydraulic engine mounts (HEMs) have the best noise, vibration and harshness (NVH) performance. Based on the third type HEM, which has an inertia track, decoupler and disturbing plate, the influences of the three hydraulic mechanisms, the length of the inertia track or the diameter of the orifice on the dynamic properties were studied experimentally. The working principles of the hydraulic mechanisms and the relationship between the dynamic properties of the three type HEMs were revealed clearly. It was discovered that the frequency-variant dynamic properties of HEMs with an inertia track or an orifice have excitation amplitude-invariant fixed points. Based on the theory of engineering hydromechanics, a nonlinear lumped parameter model (LPM) for an HEM with an inertia track was established, and an analytical solution was obtained in which the fixed point of dynamic stiffness in-phase was discovered theoretically. According to the phenomena of fixed points and the constant value of dynamic stiffness in-phase at higher bands, a new parameter identification method (PIM) was presented, which is clear in theory and is time and cost savings, the identified results are reliable. The results show that the fluid flow through an orifice can be replaced by a fluid flow through an equivalent length of inertia track. After this, a PIM for the fluid-flow local loss factor was developed. The identified results and the numerical simulations show that the reason the disturbing plate can keep the dynamic stiffness lower at higher bands is that the disturbing plate can sharply increase the quadratic fluid damping due to larger local loss, and then the resonance of the fluid flow through the decoupler channel or orifice is greatly attenuated. This conclusion is a useful attempt to explain the working principle of the disturbing plate.

1. Introduction

The powerplant is the main source of vibrations in vehicles. There are two important issues for powerplant vibration isolation [1–5]: one is the support function, which means the large amplitude vibration at lower resonance bands should be limited and reduced rapidly. This function requires the mountings to have greater stiffness and damping. The other function is noise control, which means the mountings should effectively

*Corresponding author. Tel.: +86 10 6279 5648; fax: +86 10 6278 5708.
E-mail address: fanrl@mail.tsinghua.edu.cn (R. Fan).

0022-460X/$ - see front matter © 2007 Elsevier Ltd. All rights reserved.
doi:10.1016/j.jsv.2007.04.045

Nomenclature

A_d decoupler area
A_i cross-sectional area of inertia track
A_p equivalent piston area of main rubber
b viscous damping coefficient of mount
b_i equivalent damping coefficient of inertia track, $b_i = R^2\hat{b}_i$
$\hat{b}_i$ damping coefficient induced by fluid flowing in inertia track, $\hat{b}_i = \hat{b}_{il} + \hat{b}_{id}$
$\hat{b}_{id}$ damping coefficient induced by local loss of fluid flowing at entrance and outlet of inertia track
$\hat{b}_{il}$ damping coefficient induced by loss of fluid flowing along inertia track
b_r damping coefficient of main rubber in vertical direction
D_f modified coefficient of local loss factor ξ_d
d_i hydraulic diameter of inertia track, $d_i = 4A_i/L_i$
f excitation frequency (Hz)
f_1 reaction force at top end
f_l frictional coefficient between the fluid and the wall of inertia track
f_n resonance frequency of fluid flowing in inertia track (Hz)
f_p, f_q, f_r, f_s, f_t fixed point frequency on frequency- and amplitude-variant dynamic stiffness modulus, dynamic stiffness in-phase, loss angle, dynamic stiffness out-of-phase and viscous damping coefficient
f_φ^p frequency corresponding to peak loss angle
f_ξ^p frequency corresponding to peak damping ratio
k, k' dynamic stiffness in-phase and out-of-phase, $k(\omega) = K\cos\varphi$, $k'(\omega) = K\sin\varphi$
k_l equivalent linear stiffness of the volumetric elasticity of lower chamber, $k_l = A_p^2K_l$
k_q dynamic stiffness in-phase at fixed point Q
k_{rs}, k_r static and dynamic stiffness in-phase of main rubber in vertical direction
k_u equivalent linear stiffness of the volumetric elasticity of upper chamber, $k_u = A_p^2K_u$
k_∞ dynamic stiffness in-phase at higher bands
K, K^* cross-point dynamic stiffness modulus and dynamic stiffness, $K^* = Ke^{j\varphi} = k + jk' = k(1 + j\eta) = k + j\omega b$
K_f^* dynamic stiffness induced by subsystem of inertia track fluid—upper and lower chambers
K_r, K_r^* cross-point dynamic stiffness modulus and dynamic stiffness (complex) of main rubber in vertical direction, $K_r^* = k_r + j\omega b_r$
K_{ls}, K_l static and dynamic bulk stiffness of lower chamber
K_{us}, K_u static and dynamic bulk stiffness of upper chamber
K_∞ cross-point dynamic stiffness modulus at higher bands
l_i length of inertia track
l_i' physical length of orifice
L_i wet perimeter of cross-sectional area of inertia track
m_e lumped mass of powerplant
$\hat{m}_i$ lumped mass of fluid in inertia track, $\hat{m}_i = \rho A_i l_i$
m_i equivalent mass of fluid in inertia track, $m_i = R^2\hat{m}_i$
m_r equivalent lumped mass of main rubber at top end
P_i, Q_i, R_i, S_i T_i ($i = 1$–6) fixed point on frequency- and amplitude-variant dynamic stiffness modulus, dynamic stiffness in-phase, loss angle, dynamic stiffness out-of-phase and viscous damping coefficient
p_1, p_2 fluid pressure in upper and lower chamber
R area ratio, $R = A_p/A_i$
R_d dynamic hardening coefficient of HEM, $R_d = K/K_r$
R_{ds} dynamic–static ratio of main rubber in vertical direction, $R_{ds} = k_r/k_{rs}$
Re Reynolds number of fluid flowing in inertia track, $Re = \rho|\dot{\hat{y}}_2|d_i/\mu$
R_{id}, R_{il} equivalent damping coefficient of inertia track induced by local loss factor ξ_d at entrance and outlet and by loss factor ξ_l of fluid flowing along inertia track
V_1, V_2 volume of upper and lower chambers
y_1 excitation displacement applied at the top end of mount
$\hat{y}_2$ reaction displacement of fluid in inertia track

y_2	equivalent reaction displacement of fluid in inertia track, $y_2 = \hat{y}_2/R$	ξ_l	loss factor of fluid flowing along inertia track
y_3	displacement of the lower end of mount	ξ_d	local loss factor of fluid flowing at entrance and outlet of inertia track, $\xi_d = \xi_{d1} + \xi_{d2}$
y_4	reaction displacement of decoupler		
φ	loss angle of mount	ξ_{d1}	local loss factor of fluid flowing at entrance of inertia track
φ_2	delay angle of $\hat{y}_2$ relative to y_1		
η	loss tangent (loss factor, $\tan\varphi$) of mount	ξ_{d2}	local loss factor of fluid flowing at outlet of inertia track
η_f	loss tangent resulting from dynamic stiffness of subsystem of inertia track fluid—upper and lower chambers	ξ'_d	modified local loss factor, $\xi'_d = D_f\xi_d$
		FEA	finite element analysis
λ	frequency ratio, $\lambda = \omega/\omega_n = f/f_n$	FRF	frequency response function
μ	viscosity of fluid in chambers	HEM	hydraulic engine mount
ρ	mass density of fluid in chambers	LPM	lumped parameter model
ρ_r	mass density of main rubber	NVH	noise, vibration and harshness
ω	excitation circular frequency (rad/s)	PIM	parameter identification method
ω_n	resonance frequency of fluid flowing in inertia track (rad/s)		

reduce the noise in the passenger compartment induced by small amplitude vibration of the powerplant at higher bands. This function requires the mountings to have lower stiffness and damping. These two requirements are contradictory, and the primary aim in the development of mounting technologies is to harmonize these two conflicting requirements.

Traditional rubber mounting cannot resolve the conflict because of the limitations of rubber material: its low damping cannot reduce large amplitude vibration rapidly at lower resonance bands, and so greater stiffness is needed; however, greater stiffness will result in bad noise at higher bands. On the other hand, the performance of high damping rubber is not stable and it cannot be widely used in the automotive industry now.

At present, hydraulic engine mounts (HEMs) have the best noise, vibration and harshness (NVH) performance among the passive engine mounts. The HEM with an inertia track or orifice is the first type, the one with an inertia track and decoupler is the second type, and the one with an inertia track, decoupler and disturbing plate is the third type, as shown conceptually in Fig. 1 [6–10]. Each new type HEM has inherited the former type's excellence and has overcome the former type's shortcomings in some sense.

Studies on HEMs are focused on three issues: (a) How to explain the working principles for three different types of hydraulic mechanisms. (b) How to develop a valid lumped parameter model (LPM) to accurately reflect the frequency- and amplitude-variant nonlinear dynamic properties at wider bands. (c) How to obtain or identify the parameters. The three issues are closely related. To explain the working principles correctly is the foundation for designing and developing a new HEM; a wide-band-valid LPM is a connection between the parameters and the mount's properties, and also the basis for the explanation of working principles, for parameter-sensitivity-analysis and for dynamics simulation of the whole powerplant-mounting system or the whole vehicle system; a valid LPM is always based on accurate parameters. Many studies on HEMs have been reported [1–14]; however, there are also some aspects that have not been studied or reported on, such as the ones outlined below:

(1) There are some fixed points on the frequency response function (FRF) for some damped vibration systems. For example, there are damping-invariant fixed points on the FRFs of a damped dynamic absorber and also on the transmission functions of a single degree-of-freedom (dof) damped vibration system, when the system has different damping. HEM is a typical system with damping, we knew there are fixed points on some of its dynamic properties, we want to know whether there are fixed points on all of the dynamic properties.

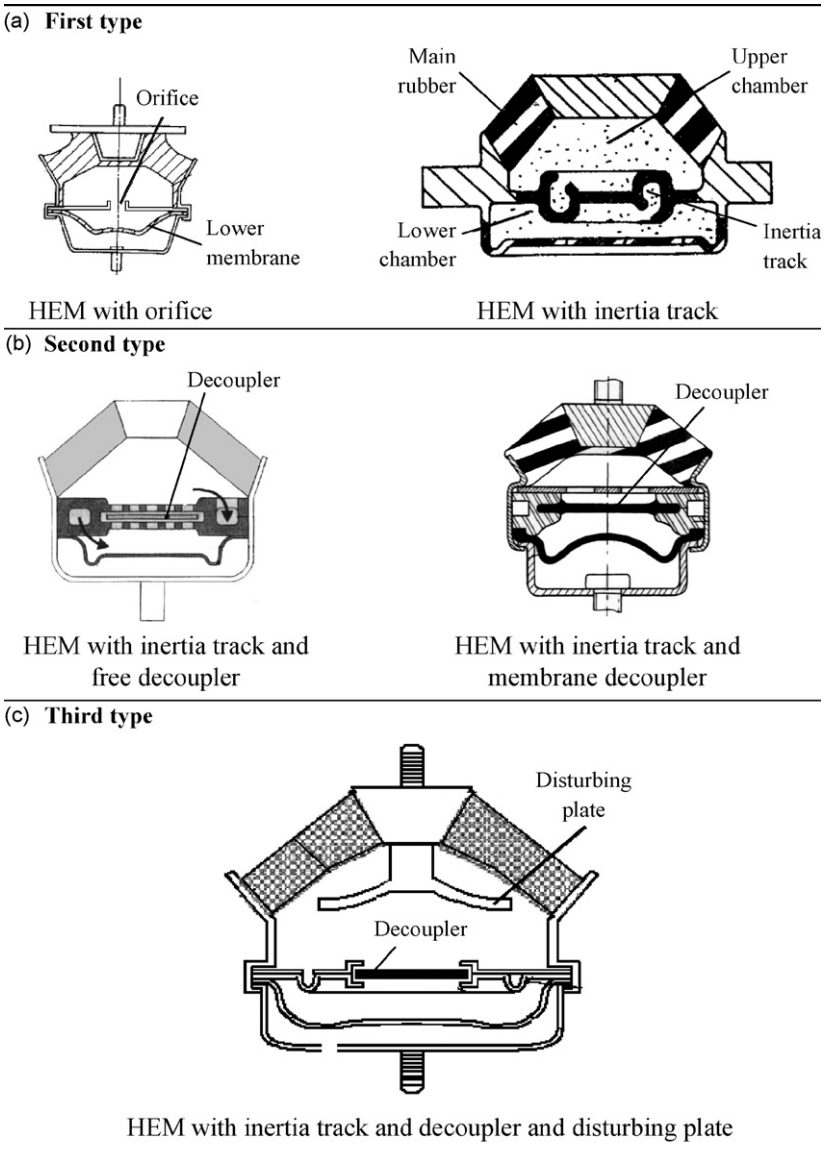

Fig. 1. Configuration schematics for the three types of hydraulic engine mounts (HEMs).

Singh et al. [1–3] have developed a linear LPM for the HEM with an inertia track and for the HEM with an inertia track and free decoupler based on whether the decoupler is or is not bottomed out. Colgate et al. [4] have also developed a linear LPM for the HEM with an inertia track and a piecewise linear LPM to incorporate the decoupler behavior for the HEM with an inertia track and free decoupler. Geisberger et al. [11] have developed a nonlinear LPM considering the linear and quadratic fluid damping, and investigated the corresponding numerical solutions. Patrick et al. [12] have conducted many experimental studies on dynamic properties. Some of their experimental results have shown the existence of the fixed points on some of the dynamic properties. In this article, it will be shown that there are fixed points on all of the dynamic properties, i.e., dynamic stiffness modulus, dynamic stiffness in-phase, loss angle, dynamic stiffness out-of-phase and equivalent damping coefficient.

(2) Generally, model parameters are obtained by taking some measurements [11,13], which requires special equipments and is time and cost consumings. The parameter identification method (PIM) is a recently

proposed method involving testing that can be carried out on a general elastomer test system, making it a time- and cost-saving method.

This method was developed and used first by Colgate et al. [4] based on the linear LPM developed by themselves. The method assumed that the equivalent piston area of the main rubber is a known parameter. Kyprianou et al. [14] also used this method to identify the parameters for the LPM constituted of a series of highly nonlinear differential equations developed by Freudenberg.

(3) The third type HEM, which has three different hydraulic mechanisms such as an inertia track, decoupler and disturbing plate, is the most complicated among the three type HEMs. Michio [10] has done qualitative experimental studies comparing the three types of HEMs, and found that the third type HEM has lower dynamic stiffness than the second type. How the disturbing plate can make the dynamic stiffness lower at higher hands is also an issue to be explained.

(4) There are many studies on the dynamic properties of HEMs; however, these results are not comparable because of their difference in geometric structures. It is necessary to do quantitative comparison based on the same structure, e.g., the same main rubber, the same upper and lower chamber and the same fluid, in order to elucidate the inheritance and development of the dynamic properties for the three type HEMs and then provide a guiding principle for HEM selection and design.

Fig. 2 shows the HEM structures discussed in this article. Its geometric and material parameters are listed in Table 1. Some changes of the inertia track are made or the combination of the three hydraulic mechanisms are reorganized. Then the influences of different hydraulic mechanisms on the dynamic properties of the HEMs are studied experimentally, the results are compared step by step to reveal the working principles of the hydraulic mechanisms and the relationship between the three type HEMs. The experimental results for HEMs with different lengths of inertia tracks or with different diameters of orifices are presented to show that all of the frequency-variant dynamic properties have fixed points under different displacement amplitude

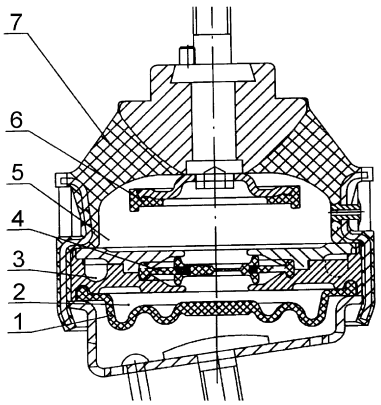

Fig. 2. A third-type HEM: 1. rubber bellow; 2. lower chamber; 3. inertia track; 4. membrane decoupler; 5. upper chamber; 6. disturbing plate; 7. main rubber.

Table 1
Geometric and material parameters of the HEM in Fig. 2

Parameter	Value	Parameter	Value
Upper-side diameter of the upper chamber d_1/mm	30.00	Length of the inertia track l_i/mm	216.59
Under-side diameter of the upper chamber d_2/mm	76.00	Density of the main rubber ρ_r/(kg/m^3)	1050.00
Cross-sectional area of the inertia track A_i/mm^2	56.90	Poisson ratio of the main rubber v	0.50
Wet perimeter of the inertia track L_i/mm	28.51	Density of the filled fluid ρ/(kg/m^3)	980.00
Hydraulic diameter of the inertia track d_i/mm	7.98	Viscosity of the filled fluid μ/(Pa.s)	0.02

excitations. And then a nonlinear LPM for HEMs with inertia track is developed based on the theory of engineering hydromechanics, an analytical solution is obtained, which shows the excitation amplitude-invariant fixed point on the frequency-variant dynamic stiffness in-phase theoretically. Lastly, a new PIM for HEMs with inertia track (or orifice) and with or without disturbing plate is designed, the identified results may be helpful to explain the effect of the disturbing plate.

2. Experimental study

2.1. Samples and experimental method

The comparability of results was the basis for this experimental study of the three type HEMs. To assure the validity and comparability of the results, first, the rubber and rubber-metal components for samples were manufactured on the same shift so as to ensure the consistency of vulcanization process conditions; secondly, no air was allowed in the chambers, because air would result in distortion and lack of repeatability of dynamic properties; thirdly, two samples were manufactured for the same configuration of HEM. The samples and the test results were considered to be valid only if the test dynamic properties of the two samples were almost the same as each other.

A total of 18 samples as listed in Table 2 were prepared. The test items, conditions [4] and data sampling requirements are listed in Table 3. During testing, the mount was excited by single frequency sinusoidal signal step by step. Then the spectra of the test time-domain signals were analyzed and the dynamic properties, i.e., dynamic stiffness K^* (complex spring rate), dynamic stiffness modulus K, dynamic stiffness in-phase (dynamic spring rate) k, loss angle φ (or loss tangent $\tan\varphi$), dynamic stiffness out-of-phase (loss rate) k' and equivalent

Table 2
Mount samples and corresponding configuration

Sample	Configuration variation relative to the HEM as shown in Fig. 2
1, 2	HEM with inertia track: the first type, without the disturbing plate; the decoupler is fixed, and the length of the inertia track is its original length $l_{i1} = 216.59$ mm
3, 4	HEM with inertia track and decoupler: the second type, without disturbing plate
5, 6	HEM with inertia track and decoupler and disturbing plate: the third type shown in Fig. 2
7, 8	Main rubber mount, without inertia track, decoupler or disturbing plate, no filled fluid
9, 10	HEM with inertia track whose length is $l_{i2} = 121.29$ mm; the other configurations are the same as samples 1 and 2
11, 12	HEM with inertia track whose length is $l_{i3} = 75.81$ mm; the other configurations are the same as samples 1 and 2
13, 14	HEM with a smaller orifice whose cross-sectional area is $A_{i4} = 144.00\,\text{mm}^2$, hydraulic diameter $d_{i4} = 10.67$ mm and physical length $l_{i4} = 13.20$ mm, without inertia track, decoupler or disturbing plate
15, 16	HEM with a larger orifice whose cross-sectional area is $A_{i5} = 785.40\,\text{mm}^2$, hydraulic diameter $d_{i5} = 31.62$ mm and physical length $l_{i5} = 15.50$ mm, without inertia track, decoupler or disturbing plate
17, 18	HEM with a larger orifice the same as samples 15 and 16 and a disturbing plate the same as samples 5 and 6, without inertia track or decoupler

Table 3
Test items and conditions for all the samples listed in Table 2

Item	Condition	Data sampling
Static compression	Compression −18 mm with velocity 10 mm/min and then release	200 sampled points
Larger amplitude at lower band (Case 1)	Static preload: compression –500 N; frequency $f = 2$–50 Hz; amplitude $A = 0.4$, 0.6, 0.8 and 1.0 mm	32 periods and 32 points per period
Smaller amplitude at higher band (Case 2)	Static preload: compression –500 N; frequency $f = 20$–200 Hz; amplitude $A = 0.05$ and 0.1.0 mm	32 periods and 32 points per period

Fig. 3. Some test samples (left) and the test rig (right).

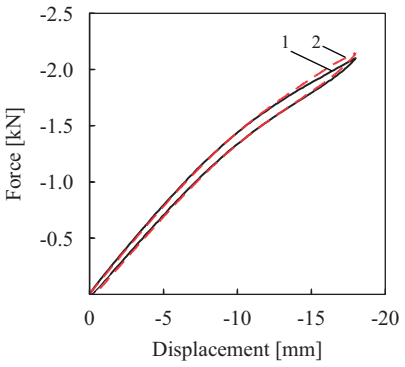

Fig. 4. Static force–displacement properties of the main rubber mount: 1. sample 7; 2. sample 8.

damping coefficient b were obtained [15]:

$$K^* = K(\cos\varphi + j\sin\varphi) = k + jk' = k(1 + j\tan\varphi) = k + j\omega b. \quad (1)$$

Tests were done on an MTS 810 Elastomer Test System. Some tested samples and the test rig are shown in Fig. 3. Transducers were calibrated before testing. Only dynamic properties in the vertical direction were tested.

2.2. Comparison between the dynamic properties of the three type HEMs and the main rubber mount

The static force–displacement properties of the two samples (samples 7 and 8 listed in Table 2) for the main rubber mount are shown in Fig. 4. It can be seen that their properties were almost the same. In fact, the static properties of all samples listed in Table 2 were consistent. These results show that the vulcanization process conditions for these samples were stable and consistent, and the static properties of the HEMs were determined only by their main rubber. The test average static stiffness of the main rubber between a compression load of 400–600 N was $k_{rs} = 149.72$ N/mm.

The comparison between the dynamic properties of the two samples with the same configuration shows that the dynamic properties under lower bands, larger amplitudes excitation (Case 1 listed in Table 3) and higher bands, smaller amplitudes excitation (Case 2 in Table 3) were also almost the same, respectively, which means the mount assemblies and their components were consistent. This allowed us to study the influences of the three different hydraulic mechanisms, i.e., inertia track, decoupler and disturbing plate, on the dynamic properties of the HEMs based on their dynamic differences, and then reveal their working principles. To make the curves are clear and legible in the following figures, only one sample's test results are shown.

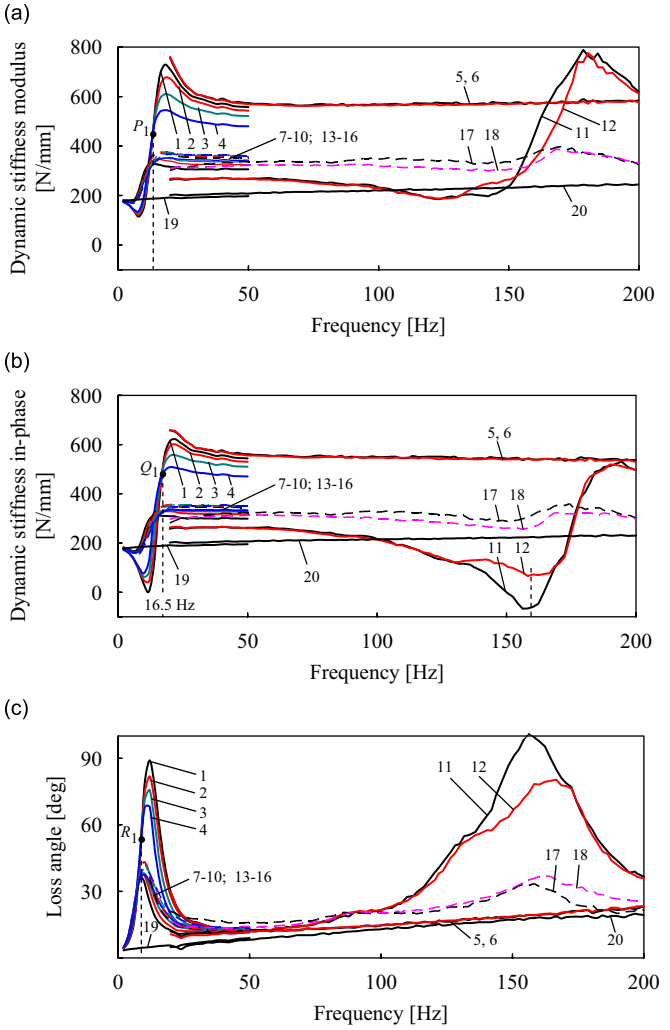

Fig. 5. Dynamic properties of four type mounts: (a) dynamic stiffness modulus, (b) dynamic stiffness in-phase, (c) loss angle. 1–4, HEM with inertia track under excitation amplitude $A = 0.4$, 0.6, 0.8 and 1.0 mm at frequency $f = 2$–50 Hz, respectively, 5–6, the same HEM under $A = 0.05$ and 0.10 mm at $f = 20$–200 Hz; 7–10, HEM with inertia track and decoupler under $A = 0.4$, 0.6, 0.8 and 1.0 mm at $f = 2$–50 Hz, 11–12, the same HEM under $A = 0.05$ and 0.10 mm at $f = 20$–200 Hz; 13–16, HEM with inertia track, decoupler and disturbing plate under $A = 0.4$, 0.6, 0.8 and 1.0 mm at $f = 2$–50 Hz, 17–18, the same HEM under $A = 0.05$ and 0.10 mm at $f = 20$–200 Hz; 19, the main rubber mount under $A = 1.0$ mm at $f = 2$–50 Hz, 20, the same mount under $A = 0.10$ mm at $f = 20$–200 Hz.

The dynamic properties of the main rubber and the three type HEMs under Cases 1 and 2 are shown in Fig. 5, which clearly shows the inheritance and development in dynamic properties.

2.2.1. *Main rubber mount*

As shown by curves 19 and 20 in Fig. 5, the dynamic stiffness modulus K_r and dynamic stiffness in-phase k_r under Cases 1 and 2 followed an almost continuously horizontal line; thus, it can be considered as a constant. The average values from all test points of the two samples were $K_r = 225.17$ N/mm (the standard deviation was 13.66 N/mm), $k_r = 217.84$ N/mm (the standard deviation was 9.15 N/mm). The dynamic–static ratio was $R_{ds} = 1.46$.

The loss angle was a continuous bias, whereas the damping coefficient b_r in the vertical direction was also a continuously horizontal line (the curves are not shown in Fig. 5) and can be considered as a constant too. As with the former averaging method, the average value was $b_r = 80.4 \times 10^{-3}$ N s/mm (the standard deviation was 9.5×10^{-3} N s/mm).

2.2.2. HEM with inertia track (the first type HEM)

As shown by curves 1–4 in Fig. 5, its dynamic properties under Case 1 are drastically frequency and amplitude variants. As the frequency increased, the lowest and peak values appeared consequently on its dynamic stiffness modulus and dynamic stiffness in-phase, and then tended to become a horizontal line; the peak loss angle decreased as the excitation amplitude increased; however, it was far larger than the one of the main rubber mount. This is the very embodiment of the larger damping of the HEM.

Under Cases 2, the dynamic stiffness modulus K_∞ and dynamic stiffness in-phase k_∞ (curves 5 and 6 in Figs. 5(a) and (b)) were almost superposed and tended to be a horizontal line, respectively, so they can be considered as amplitude invariant and constant. The average values from the test points of the two samples between 50 and 200 Hz were $K_\infty = 564.08$ N/mm (the standard deviation was 9.65 N/mm), $k_\infty = 540.09$ N/mm (standard deviation 13.45 N/mm). The ratio of K_∞ and K_r, i.e., the dynamic hardening coefficient of the HEM was $R_d = 2.51$. Its loss angle (curves 5 and 6 in Fig. 5(c)) tended to be superposed with curve 20 of the main rubber mount. This phenomenon indicated that at higher bands the damping effect of the inertia track had disappeared and the damping of the HEM was determined entirely by its main rubber, because the response of the fluid in the inertia track was roughly attenuated.

The test results showed that, the HEM with an inertia track has a much larger loss angle than the main rubber mount, which is its advantage. However, at higher bands ($f >$ the resonance frequency of the fluid in inertia track) the resistance of fluid flow through the inertia track is greater than the resilience of the main rubber. This means the fluid pressure in the upper chamber fluctuates with the excitation frequency while the fluid in the lower chamber stays under a constant pressure, and this phenomenon results in drastic dynamic hardening and consequently a higher noise level at higher bands. This is its deficiency. Adding a decoupler to the HEM with an inertia track will effectively eliminate this flaw.

2.2.3. HEM with inertia track and decoupler (the second type HEM)

Compared to drastically frequency- and amplitude-variant dynamic properties of the HEM with an inertia track under Case 1, the dynamic properties of the HEM with an inertia track and decoupler (curves 7–10 in Fig. 5) were not so drastic and converged almost together, and the peak loss angle was decreased to 38°. The decrease of the damping effect at lower bands was compensated for by lower dynamic stiffness at higher bands as shown in curves 11 and 12. The average dynamic stiffness modulus K below 160 Hz was only 260.00 N/mm and correspondingly $R_d = 1.15$, which was less than 50% of the HEM with only an inertia track. However, the fluid flowing channel through the decoupler consequentially induced another dof, resulting in more complicated dynamic behavior.

As shown in Fig. 5, the dynamic stiffness modulus K reached the second lowest value of 209.29 N/mm at 132 Hz and the second peak value of 789.11 N/mm at 180 Hz. This phenomenon was induced by the dynamic effect of the additional dof. The second peak means the HEM with an inertia track and decoupler underwent another serious dynamic hardening, $R_d = 3.50$. For a 4-cylinder in-line engine, the dynamic hardening band (150–200 Hz) corresponds to the second-order excitation frequency of the imbalanced reciprocating inertia force at rotational speeds of 4500–6000 rev/min, which is the commonly used speed for passenger cars at higher velocity. In order to reduce the noise level at higher bands, the HEM with an inertia track and decoupler must be further modified. Adding a disturbing plate to the top of the upper chamber will drastically decrease the second peak value and obtain lower dynamic stiffness on a wider band.

2.2.4. HEM with inertia track, decoupler and disturbing plate (the third type HEM)

As shown by curves 13–16 in Fig. 5, the dynamic properties of the third type HEM under Case 1 were almost the same as those of the second type HEM (curves 7–10). This means adding a disturbing plate did not have a great affect on the dynamic properties under Case 1. The second lowest value of 316.03 N/mm at 132 Hz and the second peak value of 402.38 N/mm at 170 Hz on the dynamic stiffness modulus were also found under Case 2 (curves 17 and 18 in Fig. 5(a)), nevertheless these two values had less difference than the ones of the second type HEM, and the curves tended to follow a horizontal line, and the average value was only 341.57 N/mm (the standard deviation was 29.90 N/mm), $R_d = 1.52$. These results show that the third type HEMs has inherited the advantages of the previous type, i.e., it has greater damping at lower bands, and has

also overcome the disadvantages of the previous type, i.e., it is not subject to serious second dynamic hardening. The third type HEMs are the best passive vibration isolators.

There are several noteworthy results shown in Fig. 5. First, there seems to exist some excitation amplitude-invariant fixed points on the dynamic properties of the HEM with an inertia track, for example, the point P_1 on the dynamic stiffness modulus, the point Q_1 (at 16.5 Hz) on the dynamic stiffness in-phase and the point R_1 on the loss angle. Secondly, the lowest value of dynamic stiffness in-phase may be negative and the corresponding loss angle may be larger than 90°. This is due to the dynamic effect of fluid flowing between the chambers. For an ideal spring-damping isolator with no mass, its dynamic stiffness in-phase can only be positive and its loss angle must be less than 90°.

2.3. The fixed points on dynamic properties of HEMs with inertia track and a new PIM based on the fixed points

It is an interesting phenomenon that there are excitation amplitude-invariant fixed points on the dynamic properties of the HEM with an inertia track under different amplitudes excitations. Although there are various expressions for dynamic properties, for example K^*, K, k, φ, k' and b as shown in Eq. (1), only two of them are independent. To verify whether there are fixed points on all dynamic properties of the above expressions, three types of HEMs (samples 1 and 2, 9 and 10, and 11 and 12 as listed in Table 2) were prepared and tested. The inertia tracks of the samples have different lengths ($l_{i1,\ 2,\ 3} = 216.59$, 121.29, and 75.81 mm) but the same diameter ($d_i = 7.98$ mm). The test results are shown in Fig. 6.

It can be seen clearly from Fig. 6 that the fixed points do exist on all expressions of dynamic properties, i.e., the fixed points P_i, Q_i, R_i, S_i and T_i ($i = 1, 2, 3$ for different lengths of inertia track), and the frequency of each fixed point is different when the length of the inertia track or the expression of the dynamic properties is different. Fig. 6 also clearly shows the frequency- and amplitude-variant dynamic properties and the influence of the length of the inertia track.

There is abundant information at these fixed points and a new PIM can be derived based on these fixed points and the analytical conclusions about the nonlinear LPM for HEMs with an inertia track:

(1) The analytical conclusion showed that the frequency f_q of fixed point Q on dynamic stiffness in-phase and the resonance frequency f_n of the fluid flowing in the inertia track have the following relationship (see Section 4):

$$f_n = f_q. \tag{2}$$

Therefore, the test results for f_q can be used to identify f_n. As shown in Fig. 6(b), the curve near the fixed point Q is almost perpendicular to the frequency axis. The test error of dynamic stiffness in-phase will not result in a notable change in f_q, and thus the identified f_n will have higher precision and be credible.

From fixed points Q_1, Q_2 and Q_3, which correspond to $l_{i1,\ 2,\ 3}$, we can know from Eq. (2) that the resonance frequencies $f_{n1,\ 2,\ 3}$ are 16.5, 21.5, and 27.0 Hz, respectively.

(2) The analytical conclusion about the nonlinear LPM for HEMs with an inertia track showed that the resonance frequency f_n of the fluid flowing in an inertia track is (see Eq. (18a) in Section 3.3):

$$f_n = \frac{1}{2\pi}\sqrt{\frac{A_i}{\rho l_i}(K_u + K_l)}, \tag{3}$$

where A_i is the cross-sectional area and l_i is the length of the inertia track, ρ the mass density of the fluid, and K_u and K_l the dynamic bulk stiffness of the upper and lower chambers, respectively, which denote the fluid pressure variation corresponding to a unit volume variation of the chamber and have a dimension of N/m^5.

As shown in Fig. 2, the rubber bellow is generally crimpled and so we can assume $K_l = 0$. Then K_u can be identified based on Eq. (3) from the identified f_n. Owing to higher precision of f_n, the identified K_u will consequently be precise and credible. K_u is an important parameter and is determinant for the resonance frequency f_n, the frequency of the peak loss angle f_φ^p and the dynamic hardening coefficient R_d.

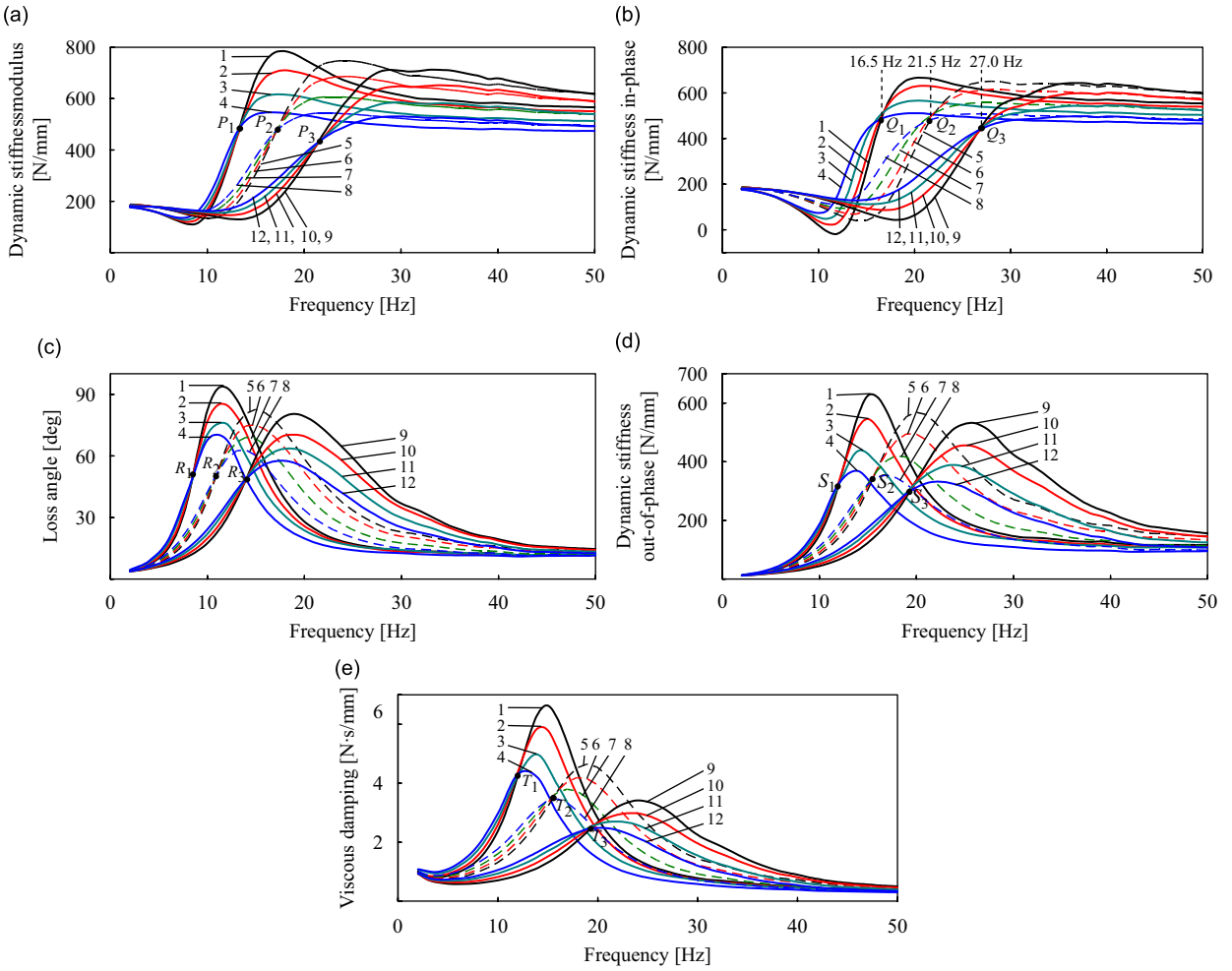

Fig. 6. Dynamic properties of three HEMs with different lengths but the same diameter $d_i = 7.98$ mm of inertia track: (a) dynamic stiffness modulus, (b) dynamic stiffness in-phase, (c) loss angle, (d) dynamic stiffness out-of-phase, (e) viscous damping coefficient. 1–4, HEM with the original inertia track of length $l_i = 216.59$ mm under excitation amplitude $A = 0.4$, 0.6, 0.8 and 1.0 mm, respectively; 5–8, $l_i = 121.29$ mm and $A = 0.4$, 0.6, 0.8 and 1.0 mm; 9–12, $l_i = 75.81$ mm and $A = 0.4$, 0.6, 0.8 and 1.0 mm.

Substituting $f_{n1,\ 2,\ 3}$ and $l_{i1,\ 2,\ 3}$ into Eq. (3), the identified $K_{u1,\ 2,\ 3}$ is 40.1, 38.1, and 37.6 GN/m^5, respectively. Regarding their average value as the dynamic bulk stiffness of the upper chamber, $K_u = 38.6$ GN/m^5.

(3) The analytical conclusion also showed when the excitation frequency f is equal to the resonance frequency f_n, the dynamic stiffness in-phase, k_q, of an HEM with inertia track can be expressed as (see Section 4):

$$k_q = k_r + A_p^2 K_u, \tag{4}$$

where A_p is the equivalent piston area of the main rubber, another important parameter for HEMs.

It can be seen from Eq. (4) that k_q is independent of the excitation amplitude. This means the dynamic stiffness in-phase under different excitation amplitudes will all pass through this point. This is the fixed point Q discovered by test results.

Using the test results for k_r, k_q and the identified result for K_u, A_p can be identified based on Eq. (4) theoretically in a sense. However, for the aforementioned reason, the curve of the dynamic stiffness in-phase near the fixed point Q is almost perpendicular to the frequency axis, which means the dynamic

stiffness in-phase is very sensitive to frequency, and a small error of excitation frequency may result in drastic variance in dynamic stiffness in-phase, and so the identified result for A_p based on Eq. (4) would no longer be precise or credible.

(4) Fortunately, the analytical conclusion again showed that the dynamic stiffness in-phase tends to be a constant at higher bands (see Eq. (33) in Section 3.3):

$$k_\infty = k_r + A_p^2 K_u. \tag{5}$$

This conclusion matches well with the test results shown by curves 5 and 6 in Fig. 5(b), which are almost superposed and tend to be horizontal lines. As a result of being horizontal lines that are almost perpendicular to the longitudinal axis, a larger variation of excitation frequency at higher bands will only result in an almost smaller variation of dynamic stiffness in-phase, k_∞, and thus the identified result for A_p based on Eq. (5) is more precise and credible than Eq. (4).

As the test results show all the curves of dynamic stiffness in-phase of the main rubber mount and the HEM with inertia track at higher bands tend to be horizontal lines, the average values of k_r and k_∞ rather than the instantaneous values can be substituted into Eq. (5). Consequently, the identified result is $A_p = 2889.47\,\mathrm{mm}^2$.

For Fig. 6 the following should be noted:

(a) From Eq. (4) it can be seen that, for the same main rubber, its dynamic stiffness in-phase and its equivalent piston area, the bulk stiffness of the upper chamber are all uniquely determined, so HEMs composed of the same main rubber and inertia track with different lengths should have a unique value of dynamic stiffness in-phase at their fixed points, for example at the points Q_1, Q_2 and Q_3 in Fig. 6(b). In fact the test results showed that the points Q_1, Q_2 and Q_3 stand nearly in a horizontal line, and the slight divergence is due to individual diversity and test error.

(b) From Eqs. (4) and (5), we have $k_\infty = k_q$, and thus the dynamic stiffness in-phase at higher bands should also stand in the same line as the fixed points Q_1, Q_2 and Q_3. The test results in Fig. 5(b) also reflect this phenomenon; the small divergence is mostly due to the test error at fixed points Q_1.

(c) The length of the inertia track, l_i, has a very complicated influence on the loss angle of an HEM with an inertia track, as shown in Fig. 6(c). With the decrease of the length of inertia track, the peak value of the loss angle decreases, the peak value frequency increases, and the peak becomes wider. To get the analytical solutions for these two variables, a quintic algebraic equation must be solved. Solving this algebraic equation theoretically would be very helpful in designing an HEM or adjusting its properties.

2.4. The fixed points on dynamic properties of the HEM only with an orifice and the PIM for the equivalent length of fluid flowing through the orifice

The HEM with an orifice is a special type of the HEM with an inertia track. Relative to the longer inertia track, the physical length of the orifice is shorter or is just an orifice in a thin board. To further verify the phenomenon about the fixed points described above, two types of samples (samples 13–16 listed in Table 2) were prepared and tested. Their orifices had different diameters (one was smaller and the other was larger) and different physical lengths.

Their test results are shown in Fig. 7 along with the results for the HEM with an inertia track (samples 1 and 2). As shown, there also were fixed points P_i, Q_i, R_i, S_i and T_i ($i = 4, 5$) on their dynamic properties, and their dynamic stiffness in-phase shown in Fig. 7(b) also tended to a constant. It can be said that fixed points are a natural phenomenon for an HEM with an inertia track. The good match between the analytical conclusions and test results indicates again the validity and universality of the nonlinear LPM and the corresponding PIM based on fixed points presented in this article.

For uniform fluid flowing in a tube, the momentum equation between two sections can be derived from the momentum conservation principle; this is the Bernoulli equation (see Eq. (6) in Section 3.1) [16]. The Bernoulli equation is also applicable to a flowing line, where the parameter l_i is the length of the flowing line and the effect of fluid jet should be considered to calculate the length of the flowing line.

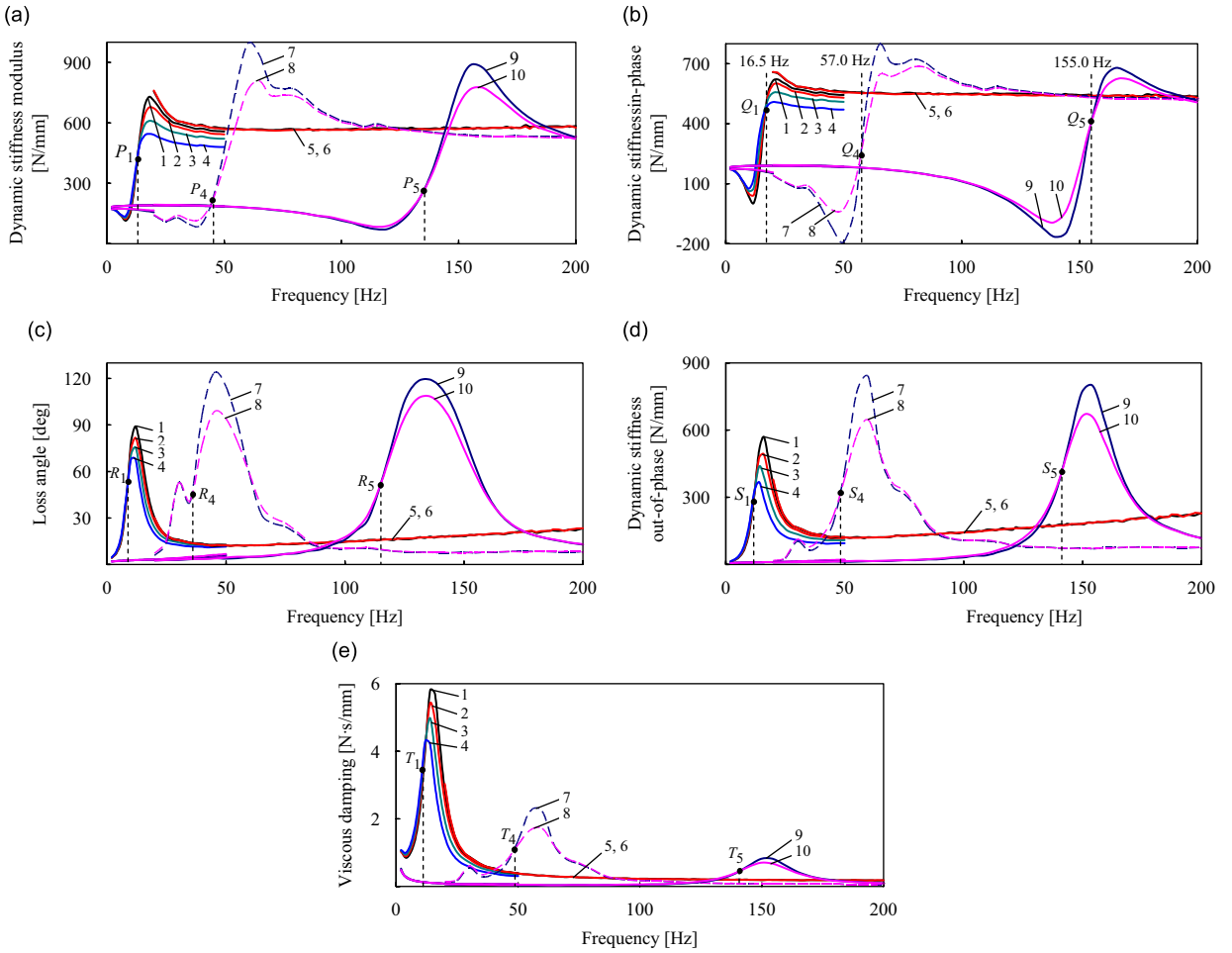

Fig. 7. Dynamic properties of three HEMs with inertia track or orifice: (a) dynamic stiffness modulus, (b) dynamic stiffness in-phase, (c) loss angle, (d) dynamic stiffness out-of-phase, (e) viscous damping coefficient. 1–4, HEM with the original inertia track of length $l_i = 216.59$ mm and diameter $d_i = 7.98$ under excitation amplitude $A = 0.4$, 0.6, 0.8 and 1.0 mm, respectively, 5–6, the same HEM under $A = 0.05$ and 0.10 mm; 7–8, HEM with a smaller orifice of $l_i = 13.20$ mm and $d_i = 10.67$ mm under $A = 0.05$ and 0.10 mm; 9–10, HEM with a larger orifice of $l_i = 15.50$ mm and $d_i = 31.62$ mm under $A = 0.05$ and 0.10 mm.

For an HEM with a long inertia track, the flowing line can be considered as the physical length of the inertia track; in other words, the effect of fluid jet can be disregarded in this case, and the good match between analytical and identified results for f_q indicates this assumption is appropriate [17].

However, for an HEM with an orifice, the flowing line may be much longer than the physical length of the orifice; in other words, the effect of fluid jet can no longer be neglected. In this case, we can regard the fluid as flowing in an inertia track with an equivalent length l_i, a different parameter from the physical length of the orifice.

The equivalent length l_i of an orifice can also be identified. Based on Eq. (2), the resonance frequency f_n can be identified from the fixed point Q_i ($i = 4$, 5), and then l_i can be determined based on Eq. (3). As shown in Fig. 7(b), $f_{q4,\,5} = 57.0$, 155.0 Hz for the smaller and larger orifice $A_{i4,\,5} = 144.00$, 785.40 mm^2; the main rubber for all samples were the same, so the formerly identified result for K_u could be used; the fluid density ρ is listed in Table 1. Consequently, the identified equivalent lengths were $l_{i4,\,5} = 44.22$ and 32.61 mm, which were markedly longer than their physical lengths 13.20 and 15.50 mm, respectively.

Based on the equivalent length, an HEM with an orifice can be modeled just like the HEM with an inertia track. So a unified nonlinear LPM for these two types of HEMs can be realized, which is helpful for dynamic simulation of powerplant-mounting system.

2.5. Function of the disturbing plate

The first type HEMs, i.e., HEMs only with an inertia track or orifice, are widely used in the automotive industry due to their simple configuration, larger damping at lower bands and lower price; however their seriously dynamic hardening at higher bands is unacceptable.

The test results in Section 2.2 show clearly the disturbing plate can make the dynamic stiffness of the third type HEMs markedly lower than the second type at higher bands.

Therefore, it is natural to suppose that the disturbing plate may also be able to reduce the dynamic hardening coefficient effectively for the first type HEMs. Consequently another type of sample, an HEM with a larger orifice and a disturbing plate (samples 17 and 18 listed in Table 2) was prepared and tested. These samples had the same orifices as samples 15 and 16 and the same disturbing plate as samples 5 and 6.

The test results are shown in Fig. 8 along with the results of the HEM only with the same orifice (samples 15 and 16). At higher bands (>150 Hz) the dynamic stiffness modulus and the dynamic stiffness in-phase of the HEM with a larger orifice and a disturbing plate (curves 3 and 4 in Figs. 8(a) and (b)) are drastically lower than the ones of the HEM only with the same orifice (curves 1 and 2), while the loss angle (shown in Fig. 8(c)) has not been changed markedly and the fixed points P_6, Q_6, R_6, S_6 and T_6 are still in existence [17] (curves not shown entirely here).

Thus, it can be concluded that adding a disturbing plate to the first type HEMs can also make their dynamic stiffness markedly lower at higher bands.

The parameter identification results (see Section 5) show that the reason the disturbing plate can significantly decrease the dynamic stiffness at higher bands is that its disturbing action on the fluid field drastically increases the quadratic nonlinear fluid damping, which consequently attenuates the resonance response of the fluid flowing through the decoupler channel or the orifice.

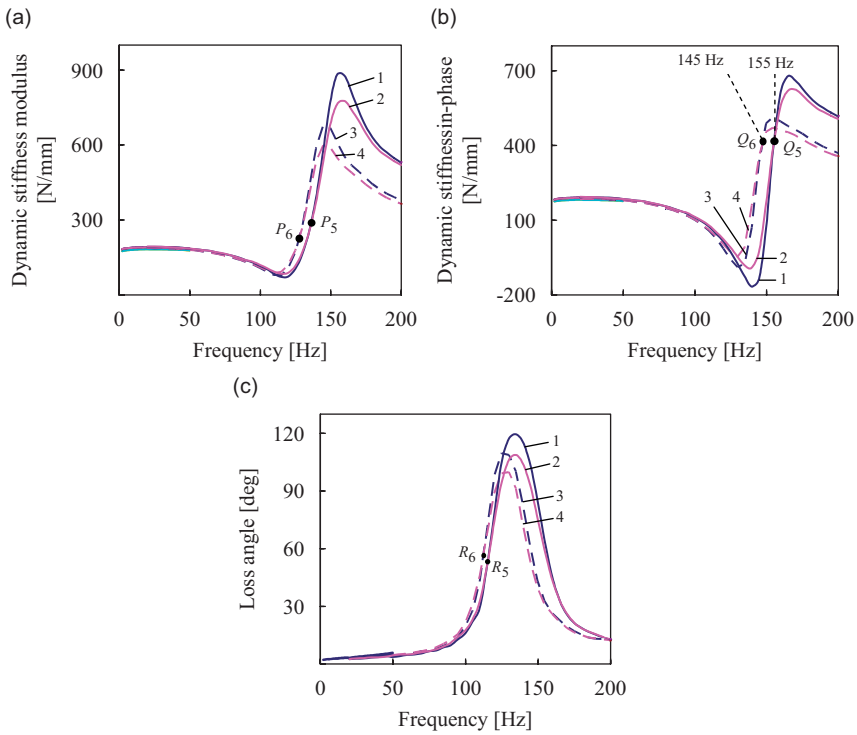

Fig. 8. Comparison between dynamic properties of HEM with an orifice and HEM with the same orifice in addition to a disturbing plate: (a) dynamic stiffness modulus, (b) dynamic stiffness in-phase, (c) loss angle. 1–2, HEM with an orifice under excitation amplitude $A = 0.05$ and 0.10 mm, respectively; 3–4, HEM with the same orifice in addition to a disturbing plate under $A = 0.05$ and 0.10 mm.

3. The nonlinear LPM for HEM with inertia track

The test results in Sections 2.3–2.5 have revealed the fixed points of the HEMs with an inertia track or an orifice (with or without a disturbing plate). In this section, a nonlinear LPM considering the linear and quadratic fluid flowing damping and its analytical solution are presented. The nonlinear LPM identifies the fixed points on dynamic stiffness in-phase, and agrees well with the experimental results. And then the proposed PIM described in Section 2.3 is discussed theoretically and systematically in Section 4.

3.1. Nonlinear LPM for vibration isolation

Referring to the schematic diagram of the HEM with an inertia track as shown in Fig. 9(a), its upper side is connected to the powerplant and the lower side to the chassis frame. The following assumptions were made: the excitation displacement at the powerplant side is y_1 and the corresponding reaction force is f_1, with the upward direction being positive; the displacement of fluid flowing relative to the inertia track is $\hat{y}_2$, with positive direction from the lower to upper chamber; the displacement at the chassis side is y_3; the fluid pressure in the upper and lower chamber is p_1 and p_2, respectively; and the force transferred to the chassis frame is f_T. These are the variables in the LPM.

The LPM uses the following parameters: dynamic stiffness in-phase and viscous damping of the main rubber in the vertical direction are k_r and b_r, its equivalent lumped mass at the upper side is m_r (including the metallic connecting piece); the equivalent piston area of the main rubber is A_p; the dynamic bulk stiffness of the upper and lower chambers is K_u and K_l; the length and cross-sectional area, wet perimeter, and hydraulic diameter of the inertia track are l_i and A_i, L_i and d_i, respectively; the loss factor of fluid flowing along the inertia track, ξ_l, is $64\mu l_i/(\rho|\dot{\hat{y}}_2|d_i^2)$ when the Reynolds number Re is less than 2320 (see Ref. [16]), the local loss factor of fluid flowing at the entrance and outlet of the inertia track is ξ_{d1} and ξ_{d2}, and the total local loss factor $\xi_d = \xi_{d1} + \xi_{d2}$. These parameters are generally measured by means of special experiments or identification.

Based on the Bernoulli equation [16] for non-stationary flow, the momentum equation in integral form for fluid flowing in an inertia track can be derived as follows:

$$\rho l_i \ddot{\hat{y}}_2 + \tfrac{1}{2}\rho(\xi_l + \xi_d)|\dot{\hat{y}}_2|\dot{\hat{y}}_2 = p_2 - p_1. \tag{6}$$

Fluid in the inertia track flows on a horizontal plane which is orthogonal to the direction of y_1 and y_3. The following continuity equations in integral form represent the fluid in the upper and lower chambers, respectively:

$$K_u(A_i\hat{y}_2 - A_p y_1 + A_p y_3) = p_1, \quad -K_l A_i \hat{y}_2 = p_2. \tag{7,8}$$

The force equilibrium equation for lumped mass m_r and the force transferred to the chassis frame f_T are as follows:

$$m_r\ddot{y}_1 + k_r(y_1 - y_3) + b_r(\dot{y}_1 - \dot{y}_3) = f_1 + A_p p_1, \tag{9}$$

$$f_T = k_r(y_1 - y_3) + b_r(\dot{y}_1 - \dot{y}_3) - A_p p_1. \tag{10}$$

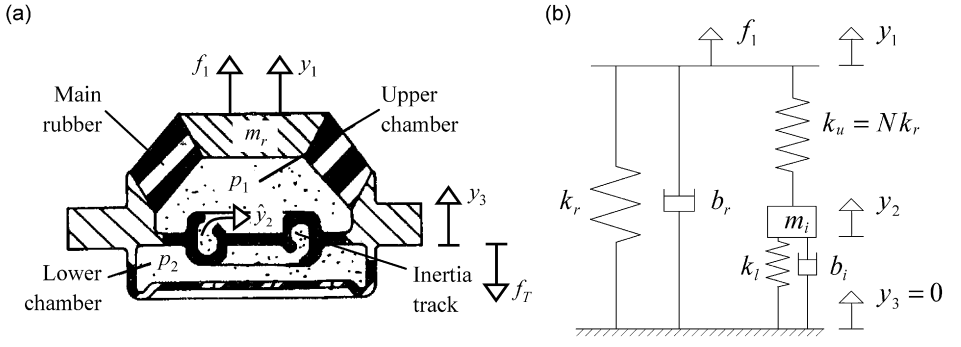

Fig. 9. Physical and equivalent mechanical models for an HEM with an inertia track: (a) physical model, (b) equivalent mechanical model.

Let $R = A_p/A_i$, $\hat{m}_i = \rho A_i l_i$, $m_i = R^2\hat{m}_i$, $\hat{b}_{il} = \rho A_i \xi_l |\dot{\hat{y}}_2|/2$, $\hat{b}_{id} = \rho A_i \xi_d |\dot{\hat{y}}_2|/2$, $\hat{b}_i = \hat{b}_{il} + \hat{b}_{id}$, $b_i = R^2\hat{b}_i$, $y_2 = \hat{y}_2/R$, $k_u = A_p^2 K_u$, $k_l = A_p^2 K_l$, $N = k_u/k_r$. Substituting these parameters into Eqs. (6)–(10) and eliminating intermediate variables p_1 and p_2, we have

$$m_r\ddot{y}_1 + b_r\dot{y}_1 + (k_r + k_u)y_1 - k_u y_2 = f_1 + (k_r + k_u)y_3 + b_r\dot{y}_3, \tag{11}$$

$$m_i\ddot{y}_2 + b_i\dot{y}_2 - k_u y_1 + (k_u + k_l)y_2 = -k_u y_3, \tag{12}$$

$$f_T = b_r\dot{y}_1 + (k_r + k_u)y_1 - k_u y_2 - (k_r + k_u)y_3 - b_r\dot{y}_3, \tag{13}$$

where k_u and k_l have a dimension of N/m and so can be regarded as the equivalent linear stiffness of bulk stiffness K_u and K_l. Usually R approximates to 50, which makes m_i be in the same order of magnitude as the mass of the powerplant [7].

3.2. Nonlinear LPM for dynamic properties

The equivalent lumped mass at the upper side, m_r, will drastically influence the drive-point dynamic properties. However, in a powerplant-mounting system, m_r is fastened to the rigid body of the powerplant, m_e; its mass contribution to the whole system can be neglected because $m_r \ll m_e$ and so we can let $m_r = 0$, and then let $y_3 = 0$ to study the dynamic properties. Based on these two assumptions, we have $f_T = f_1$ from Eqs. (11) and (13), which means the drive-point dynamic properties are equal to the cross-point ones, and the differential equations for dynamic property analysis can be written as below. The equivalent mechanical model for these equations is shown in Fig. 9(b):

$$m_i\ddot{y}_2 + b_i\dot{y}_2 - k_u y_1 + (k_u + k_l)y_2 = 0, \tag{14}$$

$$b_r\dot{y}_1 + (k_r + k_u)y_1 - k_u y_2 = f_1. \tag{15}$$

Substituting the original parameters into Eqs. (14) and (15), we have

$$\ddot{\hat{y}}_2 + \left(\frac{32\mu}{\rho d_i^2} + \frac{\xi_d}{2l_i}|\dot{\hat{y}}_2|\right)\dot{\hat{y}}_2 + \frac{A_i(K_u + K_l)}{\rho l_i}\hat{y}_2 = \frac{A_p K_u}{\rho l_i} y_1, \tag{16}$$

$$f_1 = k_r y_1 + b_r\dot{y}_1 + A_p^2 K_u y_1 - A_p A_i K_u \hat{y}_2. \tag{17}$$

Eqs. (16) and (17) are the governing equations for an HEM with an inertia track. From the first equation, $\hat{y}_2$ can be determined by excitation y_1, and then f_1 can be determined from the second equation and then p_1 and p_2 can be obtained from Eqs. (7) and (8). It can be seen that the dofs are uncoupled.

3.3. Analytical solution for nonlinear dynamic properties

As shown in Eq. (16) the fluid flowing in the inertia track is just like a single dof vibration system. The parameters in its stiffness item have the following characteristics: the geometric parameters A_i and l_i are constants; the fluid is incompressible and ρ is a constant; the test and FEA results show K_u is also a constant; K_l is smaller by two orders of magnitude than K_u due to the crimpled rubber bellow. So the stiffness item is a constant. For the parameters in its damping item, the damping induced by the loss factor of fluid flowing along the inertia track, $R_{il} = 32\mu/\rho d_i^2$, is a linear damping, and the one induced by the local loss factor at the entrance and outlet, $\xi_d|\dot{\hat{y}}_2|/2l_i$, is a quadratic nonlinear damping. Methods of multiple scales and averaging-based perturbation analytical conclusions show [18], as in the case of linear damping, that the resonance frequency is not affected by quadratic damping to its order. Therefore, for the vibration system with quadratic damping as shown in Eq. (16), its resonance frequency can be regarded as the frequency of the corresponding linear vibration system. Then the resonance frequency of fluid flowing in an inertia track can be written as below:

$$f_n = \frac{1}{2\pi}\sqrt{\frac{A_i}{\rho l_i}(K_u + K_l)}, \quad \omega_n = 2\pi f_n. \tag{18a,b}$$

Eq. (18) means the frequency is closely related to the bulk stiffness values of the upper and lower chambers, and the two bulk stiffness values have a parallel connection. Eq. (3) for PIM in Section 2.3 comes from Eq. (18) here.

Results of testing and numerical simulation show [17] that, under excitation of sinusoidal displacement y_1, the responses of p_1, p_2, $\hat{y}_2$ and f_1 are almost sinusoidal at the same frequency. Thus, the responses can be written in the following forms:

$$y_1 = Y_1 e^{j\omega t}, \quad \hat{y}_2 = \hat{Y}_2 e^{j(\omega t-\varphi_2)}, \quad f_1 = F_1 e^{j\omega t}. \tag{19}$$

where Y_1 and $\hat{Y}_2$ are positive amplitude, and φ_2 is the delay angle of $\hat{y}_2$ to y_1. Under these circumstances, the quadratic fluid damping can be regarded as an equivalent linear damping, $R_{id} = 4\xi_d \omega \hat{Y}_2/3\pi l_i$, based on the energy conservation principle. Then Eq. (16) becomes

$$\ddot{\hat{y}}_2 + \left(\frac{32\mu}{\rho d_i^2} + \frac{4\xi_d}{3\pi l_i}\omega \hat{Y}_2\right)\dot{\hat{y}}_2 + \omega_n^2 \hat{y}_2 = \frac{A_p}{\rho l_i} K_u y_1. \tag{20}$$

Substituting y_1, $\hat{y}_2$ and f_1 from Eq. (19) into Eqs. (20) and (17), we obtain

$$(\omega_n^2 - \omega^2)\hat{Y}_2 e^{-j\varphi_2} + j\omega\left(\frac{32\mu}{\rho d_i^2} + \frac{4\xi_d}{3\pi l_i}\omega \hat{Y}_2\right)\hat{Y}_2 e^{-j\varphi_2} = \frac{A_p}{\rho l_i} K_u Y_1, \tag{21}$$

$$F_1 = k_r Y_1 + j\omega b_r Y_1 + A_p^2 K_u Y_1 - A_p A_i K_u \hat{Y}_2 e^{-j\varphi_2}. \tag{22}$$

The FRF of fluid flowing in inertia track can be written in the form below from Eq. (21):

$$H_f = \frac{\hat{Y}_2}{Y_1} e^{-j\varphi_2} = \frac{A_p}{A_i}\frac{K_u}{K_u + K_l}\frac{1}{1 - \lambda^2 + j(C\lambda/\omega_n + D\hat{Y}_2\lambda^2)}, \tag{23}$$

where $C = 32\mu/\rho d_i^2$, $D = 4\xi_d/3\pi l_i$, $\lambda = f/f_n = \omega/\omega_n$.

As shown by Eq. (23) the expression of H_f has an unknown variable, $\hat{Y}_2$, which can be solved by the following searching method: for a given excitation amplitude Y_1, increase $\hat{Y}_2$ from zero gradually and compute the corresponding H_f. If $|H_f|Y_1 = \hat{Y}_2$, then $\hat{Y}_2$ can be regarded as the response amplitude of $\hat{y}_2$ and H_f as the frequency response. The searched curve for $Y_1 = 1.0$ mm, $f = 15$ Hz is shown in Fig. 10. Numerical simulation-based experiments show that the searched curves for other excitation amplitudes and frequencies are similar to Fig. 10, which means the solution for $\hat{Y}_2$ has good properties and the searching method can guarantee the numerical precision and the reliability of $\hat{Y}_2$ and H_f [17]. The calculated amplitude- and phase-frequency response characteristics of fluid flowing in an inertia track are shown in Fig. 11, where the delay angle of 90° indicates the phase resonance when the excitation frequency is equal to the resonance frequency f_n.

Substituting Eq. (23) into Eq. (22), the dynamic stiffness can be written in the form

$$K^* = k + jk' = F_1/Y_1 = K_r^* + K_f^*, \tag{24}$$

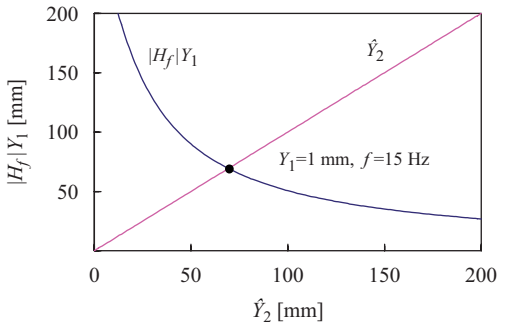

Fig. 10. The search results for displacement–response amplitude for fluid flowing in inertia track.

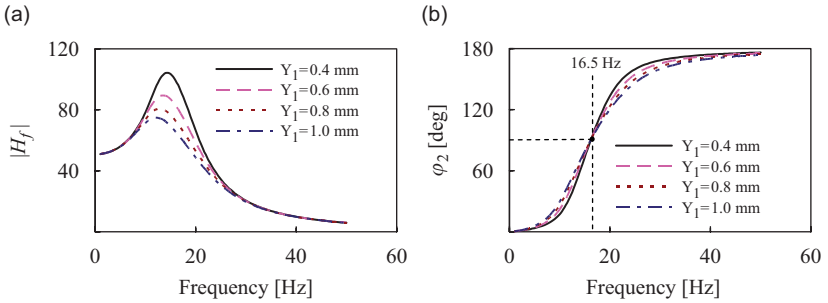

Fig. 11. The frequency response properties of fluid flowing in inertia track: (a) amplitude, (b) phase.

where $K_r^* = k_r + j\omega b_r$ is dynamic stiffness of the main rubber, and $K_f^* = A_p^2 K_u - A_p A_i K_u H_f$ is dynamic stiffness induced by the subsystem of inertia track fluid and chambers.

Based on Eq. (24), the dynamic properties of an HEM with an inertia track can be investigated theoretically:

(1) $\lambda \to 0$

Considering $K_l \ll K_u$ leads to

$$H_{f0} \approx A_p/A_i, \quad K_{f0}^* \approx 0, \tag{25,26}$$

$$K_0^* = k_0 + jk_0', \quad k_0 = k_r, \quad k_0' = 0, \tag{27,28,29}$$

where the subscript $_0$ indicates the corresponding value at $f = 0$ Hz.

As shown in Eq. (25), H_{f0} is a positive real number, which means $\hat{y}_2$ and y_1 are in-phase and the fluid pumped by the piston area of the main rubber is pumped into the lower chamber in-phase, and there is no pressure fluctuation in the chambers. Therefore, the dynamic stiffness of the HEM is contributed mainly by the main rubber. This conclusion agrees well with the experiment.

(2) $\lambda \to \infty$

$$H_{f\infty} \to 0, \quad K_{f\infty}^* = A_p^2 K_u, \tag{30,31}$$

$$K_\infty^* = k_\infty + jk_\infty', \quad k_\infty = k_r + A_p^2 K_u, \quad k_\infty' = \omega b_r, \tag{32,33,34}$$

where the subscript $_\infty$ indicates the corresponding value at higher bands ($(f \gg f_n)$). Eq. (5) for PIM in Section 2.3 comes from Eq. (33) here.

As shown in Eq. (30), the displacement response of fluid flowing in inertia track is drastically attenuated and the connection between the upper and lower chambers through the inertia track is cut off at higher bands. Under these circumstances, the fluid pumped by the piston area of the main rubber is accommodated entirely by the upper chamber due to its elasticity of bulk, thus leading to pressure fluctuation. As shown in Eq. (31), the value of $A_p^2 K_u$ can be regarded as the equivalent linear stiffness of the volumetric elasticity of the upper chamber, which indicates the comprehensive effect of the piston area and the bulk stiffness and also indicates the increment of dynamic stiffness at higher bands.

As shown in Eq. (33), the dynamic stiffness in-phase at higher bands is a superimposition of k_r and $A_p^2 K_u$. Results of testing and FEA show that the parameters k_r, A_p and K_u can be regarded as constant [17], so k_∞ tends to be a constant too. This analytical conclusion matches well with the test results shown in Fig. 5(b), in which the curves of dynamic stiffness in-phase become a horizontal line at higher bands.

(3) $\lambda = 1$,

$$H_{f1} = \frac{\hat{Y}_2}{Y_1} e^{-j\varphi_2} = -j \frac{A_p}{A_i} \frac{K_u}{K_u + K_l} \frac{\omega_n}{C + \omega_n D \hat{Y}_2}. \tag{35}$$

Because Y_1 and $\hat{Y}_2$ are positive real numbers, and then H_{f1} is a purely imaginary number that is negative, then φ_2 must be $\pi/2$ and the vibration is designated as phase resonance when the excitation frequency is the resonance frequency of the fluid. According to the fact that the real and imaginary parts on both sides of the equal sign are equal, respectively, we obtain

$$\omega_n D\hat{Y}_2^2 + C\hat{Y}_2 - \omega_n E Y_1 = 0, \tag{36}$$

where $E = A_p K_u / A_i(K_u + K_l)$.

Solving Eq. (36), considering that $\hat{Y}_2$ is a positive real number, we obtain

$$\hat{Y}_2 = \frac{-C + \sqrt{C^2 + 4\omega_n^2 DE Y_1}}{2\omega_n D}. \tag{37}$$

Substituting $\hat{Y}_2$ from Eq. (37) into Eq. (35) and then into Eq. (24), we obtain

$$H_{f1} = -j\frac{2\omega_n E}{C + \sqrt{C^2 + 4\omega_n^2 DE Y_1}}, \quad K_{f1}^* = A_p^2 K_u(1 + j\eta_f), \tag{38,39}$$

$$K_1^* = k_1 + jk_1', \quad k_1 = k_r + A_p^2 K_u, \quad k_1' = \omega b_r + A_p^2 K_u \eta_f, \tag{40,41,42}$$

$$\varphi_1 = \arctan\left(\frac{\omega b_r + A_p^2 K_u \eta_f}{k_r + A_p^2 K_u}\right), \tag{43}$$

$$\eta_f = \frac{2(K_u/(K_u + K_l))\sqrt{A_i/\rho l_i(K_u + K_l)}}{(32\mu/\rho d_i^2) + \sqrt{(32\mu/\rho d_i^2)^2 + 4(4\xi_d/3\pi l_i)(A_p/\rho l_i)K_u Y_1}}, \tag{44}$$

where the subscript $_1$ indicates the corresponding value at $f = f_n$.

As shown in Eqs. (43) and (44), some parameters can be selected to adjust the delay angle φ_1 as follows:

(a) Viscosity of the liquid, μ : decreasing μ can augment φ_1. Kazuto et al. [19] used four types of fluid, whose viscosity was decreased gradually by one order of magnitude from 1.693×10^{-3} to 1.765, to optimize the vibration isolation performance of the powerplant-mounting system and obtained a better result. This was accomplished by the effect of viscosity.

(b) Hydraulic diameter of the inertia track, d_i: for the same cross-sectional area of the inertia track, A_i, the larger the hydraulic diameter, the larger the loss angle. This is the reason that the cross-sectional area is usually in the shape of a circle.

(c) Excitation displacement amplitude, Y_1: the smaller the Y_1, the larger the η_f and then the larger the φ_1. This is the fundamental reason that the HEM with an inertia track has amplitude-variant dynamic properties. This conclusion agrees well with the test results shown in Fig. 6(c).

(d) Length of the inertia track, l_i: this parameter has a very complicated influence on the loss angle of an HEM with an inertia track, as shown in Fig. 6(c). From Eq. (44), it can be seen that the parameter l_i is in both the denominator and the numerator, and it is also related to the resonance frequency of fluid flowing in inertia track shown in Eq. (18a), whereas the parameters μ, d_i and Y_1 are just in either the denominator or the numerator and they are independent of the resonance frequency. This phenomenon results in a complicated influence on the loss angle. An advanced theoretical explanation for the relationship between the analytical results of Eqs. (43) and (44) and the experimental results shown in Fig. 6(c) should be obtained from further study. It should be noted that the parameter l_i is mainly used to adjust the resonance frequency of fluid flowing in an inertia track or adjusting the peak value frequency of the loss angle, so that the dynamic properties of the mount can match well with those of the powerplant-mounting system.

4. Parameter identification method based on the fixed points: theory

By comparing Eqs. (33) and (41) we know that $k_1 = k_\infty = k_r + A_p^2 K_u$. Because k_∞ tends to be a constant, k_1 is also a constant (i.e., amplitude invariant), which means the frequency-variant dynamic stiffness in-phase under different amplitude excitations will intersect at the resonance frequency f_n and have the value of $k_r + A_p^2 K_u$. The intersection point is the fixed point Q shown in the experimental results in Fig. 6(b).

The good match between analytical and experimental results shows the correctness of the LPM and the validity of the assumptions for its parameters. A new PIM can be developed based on the fixed points Q and the phenomena of k_∞ being constant.

Setting the excitation frequency at fixed point Q as f_q, and the corresponding dynamic stiffness in-phase as k_q, then we have $k_q = k_r + A_p^2 K_u$ and $f_q = f_n$ at fixed point Q. This is the theoretical basic for Eqs. (4) and (2) used in Section 2.3 for PIM.

Based on Eqs. (2)–(5), we can identify the bulk stiffness K_u, the equivalent piston area A_p and the equivalent length l_i of fluid flowing through an orifice, as described in Sections 2.3 and 2.4.

5. Further study on the function of the disturbing plate

The experimental and fluid–solid interaction FEA results show that the fluid flowing in the inertia track is a laminar flow at 0–200 Hz. For the nonlinear LPM developed here, the loss factor along the inertia track, ξ_l, is computed based on its laminar formulation and can reflect its damping effect exactly.

The local loss factor is highly dependent on the geometric configuration of the entrance and outlet. For a small outlet on a large vessel wall, the local loss factors ξ_{d1} and ξ_{d2} can be set to 0.5 and 1.0, respectively [16]. However, for an HEM, its inertia track has a sharp bend at the entrance and outlet, and the fluid jet will result in more energy loss. Under this case, the local loss factors ξ_{d1} and ξ_{d2} with the former values will not reflect the damping effect exactly and therefore must be modified. The damping induced by the local loss factor, ξ_d, is a quadratic nonlinear damping. Colgate [4] and Geisberger et al. [11] introduced quadratic nonlinear damping to reflect the damping effect of fluid flowing through the channel of the decoupler and their calculations agreed with experimental results. So we can also introduce a modified coefficient to study the damping effect induced by the local loss factor. Setting the modified coefficient to be D_f, the modified local loss factor becomes

$$\xi_d' = D_f \xi_d, \tag{45}$$

where $\xi_d = \xi_{d1} + \xi_{d2} = 0.5 + 1.0 = 1.5$.

The parameter D_f can be identified from the experimental results, which will disclose the effect of the disturbing plate.

Substituting ξ_d' from Eq. (45) into Eq. (6), we can see all the analytical conclusions for $\lambda = 0$ and ∞ and the analytical dynamic stiffness in-phase for $\lambda = 1$ are independent of ξ_d; however, the dynamic stiffness out-of-phase for $\lambda = 1$, being dependent on ξ_d and excitation amplitude Y_1, will become

$$k_1' = \omega b_r + A_p^2 K_u \frac{2\omega_n K_u/(K_u + K_l)}{C + \sqrt{C^2 + 4D_f D(A_p/\rho l_i) K_u Y_1}}. \tag{46}$$

This equation can be rewritten as

$$4D_f D(A_p/\rho l_i) K_u Y_1 = G^2 - 2GC, \tag{47}$$

where $G = (2A_p^2 K_u(K_u/(K_u + K_l))\omega_n)/(k_1' - \omega b_r)$.

As shown in Eq. (47), D_f can be identified from the experimental results of k_1' under different excitation amplitudes by the least squares method.

For an HEM with only an orifice, the identified result for D_f indicates the local loss induced by the entrance and outlet, while for an HEM with both an orifice and disturbing plate, D_f indicates the total local loss induced by the entrance, outlet and the disturbing plate. The difference will indicate the quantity of loss induced by the disturbing plate.

The identified results of D_f for four different types of channels (i.e. inertia track, smaller orifice, larger orifice, larger orifice with disturbing plate) are listed in Table 4. It can be seen that the modified coefficient D_f

Table 4
Identified results of modified coefficient of the local loss factor for different types of HEMs

Type of HEM (channel type)	Modified coefficient D_f	The experimental data used
HEM with an inertia track	2.74	All data of Samples 1 and 2, 9 and 10 and 11 and 12 under excitation amplitude $A = 0.4$, 0.6, 0.8 and 1.0 mm
HEM with a smaller orifice	10.62	All data of Samples 13 and 14 under excitation amplitude $A = 0.05$ and 0.10 mm
HEM with a larger orifice	46.50	All data of Samples 15 and 16 under excitation amplitude $A = 0.05$ and 0.10 mm
HEM with a larger orifice and a disturbing plate	95.91	All data of Samples 17 and 18 under excitation amplitude $A = 0.05$ and 0.10 mm

is just 46.50 for the HEM with only a larger orifice, whereas it is 95.91 for the HEM with the same orifice and a disturbing plate. So the disturbing plate can cause the local loss factor to be almost doubled, consequently causing the local loss-induced damping effect to increase drastically.

6. Simulations

Based on the analytical conclusions, Eq. (24), and the parameters identified in this article, the dynamic properties for the test samples, i.e., the HEM with an inertia track, the HEM with a smaller orifice, the HEM with a larger orifice and the HEM with a larger orifice and a disturbing plate, were simulated and compared with the experimental results shown in Figs. 12–16.

The comparison shown in Fig. 12 is for the dynamic stiffness modulus, dynamic stiffness in-phase and loss angle of the HEM with a smaller orifice. The simulation results agree well with the experimental ones at less than 200 Hz and exactly reflect the fixed points, the constant dynamic stiffness values at higher frequencies and the loss angle.

The comparison shown in Figs. 13 and 14 is for the dynamic stiffness in-phase and loss angle of the HEM with the original inertia track at lower bands (2–50 Hz) and higher bands (50–200 Hz), respectively. It can be seen that the simulated loss angle at lower bands and the dynamic stiffness in-phase at higher bands agree well with the experimental results; the simulated dynamic stiffness in-phase at lower bands and the loss angle at higher bands agree with the tendency observed in the experimental results.

In Sections 2.2 and 2.5, it is shown from the experimental results that the serious dynamic hardening phenomenon at higher bands is induced by the resonance of the fluid flowing through the decoupler channel or the orifice, and that the dynamic hardening effect can be reduced drastically by adding a disturbing plate to the top of the upper chamber.

Then in Section 5 it is shown from the parameters identified that the disturbing plate can nearly double the modified coefficient D_f and so the local loss factor ξ'_d is also almost doubled (shown in Table 4), consequently causing the local loss induced damping effect to increase drastically.

Thus, it may be concluded that the reason the disturbing plate can make the dynamic stiffness markedly lower at higher bands is that its disturbing action on the fluid field enhances the turbulent flow, enlarges the energy loss, causes the quadratic fluid damping to increase drastically, and then attenuates the resonance response of the fluid flowing through the decoupler channel or the orifice.

To verify and repeat the conclusion about the function of the disturbing plate by simulation, the dynamic properties for the samples, i.e., the HEM with a larger orifice (samples 15 and 16) and the HEM with a larger orifice and a disturbing plate (samples 17 and 18), were simulated and compared with their experimental results, as shown in Figs. 15 and 16. It can be seen that the simulated dynamic stiffness modulus at higher bands for the HEM with a larger orifice and a disturbing plate (curves 1 and 2 in Fig. 16) are indeed much lower than those for the HEM without the disturbing plate (curves 1 and 2 in Fig. 15).

A series of numerical-simulation-based tests showed that the larger the local loss factor ξ'_d (i.e., the larger the modified coefficient D_f or the larger the quadratic nonlinear fluid damping), the lower the dynamic stiffness at higher bands.

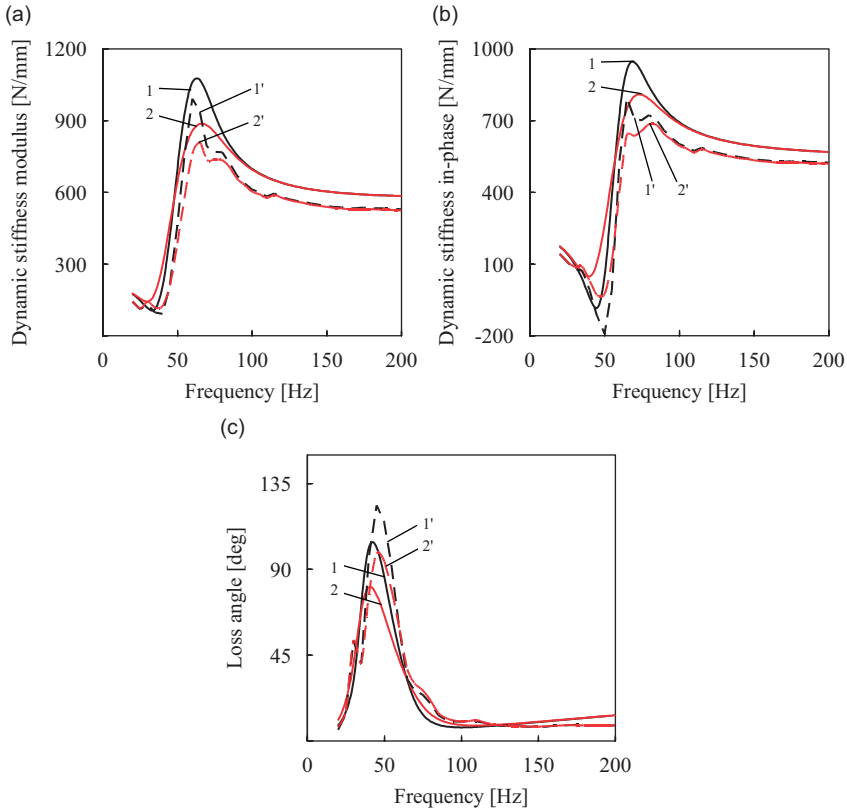

Fig. 12. Comparison between simulation and experiment for HEM with a smaller orifice (samples 13 and 14 listed in Table 2): (a) dynamic stiffness modulus, (b) dynamic stiffness in-phase, (c) loss angle. 1–2, simulation with excitation amplitude $A = 0.05$ and 0.10 mm, respectively; 1′–2′, experiment under $A = 0.05$ and 0.10 mm.

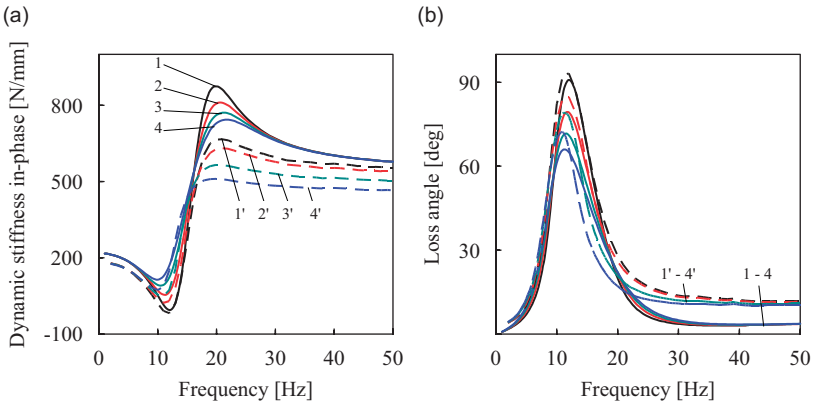

Fig. 13. Comparison between simulation and experiment for HEM with the original inertia track (samples 1 and 2 listed in Table 2) at $f = 2$–50 Hz: (a) dynamic stiffness in-phase. (b) loss angle. 1–4, simulation with excitation amplitude $A = 0.4$, 0.6, 0.8 and 1.0 mm, respectively; 1′–4′, experiment under $A = 0.4$, 0.6, 0.8 and 1.0 mm.

The simulation results agree well with the tendency observed in the experimental results, so it can be said that the conclusion about the function of the disturbing plate is reasonable and it is a useful attempt to understand the disturbing plate.

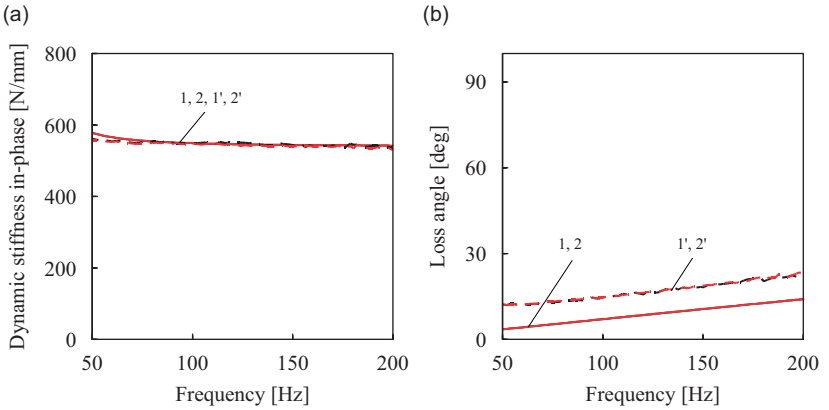

Fig. 14. Comparison between simulation and experiment for HEM with the original inertia track (samples 1 and 2 listed in Table 2) at $f = 50$–200 Hz: (a) dynamic stiffness in-phase, (b) loss angle. 1–2, simulation with excitation amplitude $A = 0.05$ and 0.10 mm, respectively; 1′–2′, experiment under $A = 0.05$ and 0.10 mm.

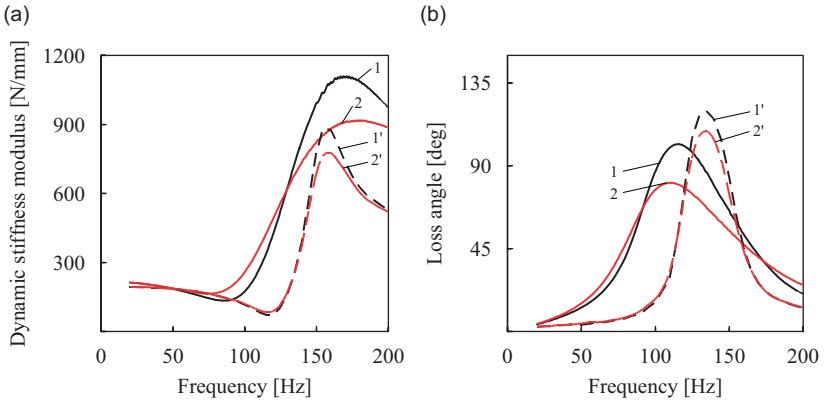

Fig. 15. Comparison between simulation and experiment for HEM with a larger orifice (samples 15 and 16 listed in Table 2) at $f = 20$–200 Hz: (a) dynamic stiffness modulus, (b) loss angle. 1–2, simulation with excitation amplitude $A = 0.05$ and 0.10 mm, respectively; 1′–2′, experiment under $A = 0.05$ and 0.10 mm.

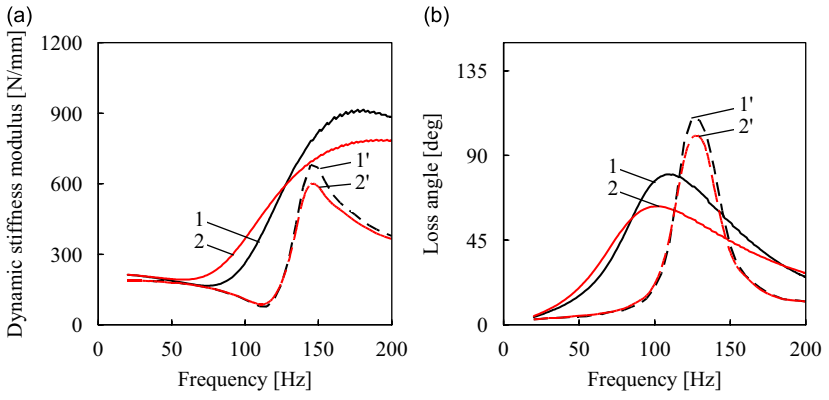

Fig. 16. Comparison between simulation and experiment for HEM with a larger orifice and a disturbing plate (samples 17 and 18 listed in Table 2) at $f = 20$–200 Hz: (a) dynamic stiffness modulus, (b) loss angle. 1–2, simulation with excitation amplitude $A = 0.05$ and 0.10 mm, respectively; 1′–2′, experiment under $A = 0.05$ and 0.10 mm.

The discrepancies between the simulation and experimental results can be attributed to the following: experimental error in measured data; general approximation made with the lumped parameters assumption, in which all of the parameters are considered as linear; approximation of the local loss factor, which is assumed to be independent of the excitation amplitude and frequency; and approximation of the loss factor of fluid flowing along an inertia track, which is calculated based on the assumption that the wall of the inertia track is smooth.

7. Conclusions

Comparison of the experimental results indicates clearly the influence of different hydraulic mechanisms on the dynamic properties of HEMs. Inertia tracks can only provide large damping at lower frequencies, at higher frequencies their damping effect disappears. Decouplers can decrease the dynamic stiffness at middle bands (40–160 Hz), but they cause severe secondary dynamic hardening due to the resonance of the fluid flowing through the decoupler channel. Disturbing plates can provide lower dynamic stiffness at wider bands (only tested at 40–200 Hz) and thus the third type HEM with an inertia track, decoupler and disturbing plate is the best passive isolator. These conclusions should provide useful guidance for the selection and design of HEMs.

The fixed points are discovered experimentally on all of the frequency-variant dynamic properties of an HEM with an inertia track or orifice under excitations of various displacement amplitude. The frequencies of the fixed points are different when the lengths of the inertia track are different; the frequencies are also different for different expressions of dynamic properties.

The analytical solution of the nonlinear LPM for an HEM with an inertia track, which is based on the theory of engineering hydromechanics, also indicates theoretically the existence of the fixed point on the dynamic stiffness in-phase.

Based on the fact that the analytical results match well with the experimental ones and according to the frequency of the fixed point and the constant value of dynamic stiffness in-phase at higher bands, a new PIM for HEMs is presented. The new PIM is clear in theory and saves time and money. The results are proven to be reliable.

The identified results show that a disturbing plate drastically increases the quadratic nonlinear fluid damping, and the numerical simulations show that the larger the quadratic damping, the lower the dynamic stiffness at higher bands. Thus, it can be concluded that the main function of the disturbing plate is to enhance the turbulent flow, enlarge the energy loss and damping effect and then to restrain the resonance response of the fluid flowing through the decoupler channel or orifice.

How to discover the fixed points analytically on other expressions of dynamic properties besides the dynamic stiffness in-phase requires further study, which may lead to the discovery of a new heuristic method for nonlinear parameter identification of HEMs.

The discrepancies between the simulation and experimental results can be attributed to experimental error in measured data and the approximation made with the lumped parameters assumption. To predicate the dynamic properties at higher bands accurately, further work should be conducted to establish a finer model for fluid flows that considers turbulence.

Acknowledgments

We gratefully acknowledge the research support from the Chinese Ministry of Education, Tsinghua University, and the Toyota Motor Corporation. We are also grateful to the Zhongding Sealing Parts Co., Ltd., PR China for making the experimental studies possible by providing the MTS Elastomer Test System and components and assembling all the mount samples.

References

[1] R. Singh, G. Kim, P.V. Ravindra, Linear analysis of automotive hydro-mechanical mount with emphasis on decoupler characteristics, *Journal of Sound and Vibration* 158 (2) (1992) 219–243.

[2] G. Kim, R. Singh, A study of passive and adaptive hydraulic engine mount systems with emphasis on non-linear characteristics, *Journal of Sound and Vibration* 179 (3) (1995) 427–453.
[3] H. Adiguna, M. Tiwari, R. Singh, H.E. Tseng, D. Hrovat, Transient response of a hydraulic engine mount, *Journal of Sound and Vibration* 268 (2) (2003) 217–248.
[4] J.E. Colgate, C.T. Chang, Y.C. Chiou, W.K. Liu, L.M. Keer, Modeling of a hydraulic engine mount focusing on response to sinusoidal and composite excitations, *Journal of Sound and Vibration* 184 (3) (1995) 503–528.
[5] A.K.W. Ahmed, M.M. Haque, S. Rakheja, Nonlinear analysis of automotive hydraulic mounts for isolation of vibration and shock, *International Journal of Vehicle Design* 22 (1) (1999) 116–128.
[6] B. Marc, A new generation of engine mounts, *SAE Transactions* 840259, 1984.
[7] E.C. Patrick, H.T. Gerd, Hydraulic engine mount characteristics, *SAE Transactions* 840407, 1984.
[8] M. Clark, Hydraulic engine mount isolation, *SAE Transactions* 851650, 1985.
[9] E.I. Rivin, Passive engine mounts—some directions for further development, *SAE Transactions* 850481, 1985.
[10] T. Michio, F. Yoshiki, K. Motohiro, New technology of antivibration rubber products for automobiles, *Automotive Technology* 44 (12) (1990) 24–30 (in Japanese).
[11] A. Geisberger, A. Khajepour, F. Golnaraghi, Non-linear modelling of hydraulic mounts: theory and experiment, *Journal of Sound and Vibration* 249 (2) (2002) 371–397.
[12] E.C. Patrick, H.T. Gerd, Hydraulic engine mount characteristics, *SAE Transactions* 840407, 1984.
[13] G. Kim, R. Singh, Nonlinear analysis of automotive hydraulic engine mount, *Journal of Dynamic Systems, Measurement, and Control—Transactions of the ASME* 115 (1993) 482–487.
[14] A. Kyprianou, J. Giacomin, K. Worden, M. Heidrich, J. Böcking, Differential evolution based identification of automotive hydraulic engine mount model parameters, *Proceedings of the Institution of Mechanical Engineers Part D—Journal of Automobile Engineering* 214 (D3) (2000) 249–264.
[15] SAE Recommended Practice SAE J1085 NOV95, Test for dynamic properties of elastomeric isolators, 1995, p. 11.
[16] W. Pan, *Engineering Hydromechanics*, Tsinghua University Press, Beijing, 1988 (in Chinese).
[17] R. Fan, Research on Vibration Modes Decoupling of Automotive Power Plant and Dynamic Characteristics of Hydraulically Damped Rubber Mount, PhD Thesis, Tsinghua University, 2005 (in Chinese).
[18] A.H. Nayfeh, D.T. Mook, *Nonlinear Oscillations*, Wiley, New York, 1979.
[19] S. Kazuto, S. Katsuml, N. Akio, I Masao, D. Kazuhlro, Optimum design method for hydraulic engine mounts, *SAE Transactions* 911055, p. 19.